Cellular Signalling 62 (2019) 109325

Contents lists available at ScienceDirect

Cellular Signalling

journal homepage: www.elsevier.com/locate/cellsig

Up-regulation of ANXA1 suppresses polymorphonuclear neutrophil infiltration and myeloperoxidase activity by activating STAT3 signaling pathway in rat models of myocardial ischemia-reperfusion injury

Can Zhao[a], Beibei Zhang[b], Jing Jiang[c], Yongliang Wang[a], Yongquan Wu[d,*]

[a] Department of Cardiology, Beijing Friendship Hospital, Capital Medical University, Beijing 100050, PR China
[b] Beijing Health Vocational College, Beijing 101101, PR China
[c] Department of Cardiology, The 971st Hospital of Chinese People's Liberation Army Navy, Qingdao 266071, PR China
[d] Department of Cardiology, Beijing Anzhen Hospital, Capital Medical University, Beijing 100029, PR China

ARTICLE INFO

Keywords:
Myocardial ischemia-reperfusion injury
ANXA1
STAT3 signaling pathway
Polymorphonuclear neutrophil infiltration
Myeloperoxidase activity
Inflammation

ABSTRACT

Myocardial ischemia-reperfusion injury (MIRI) is recognized as a major cause of morbidity and mortality which is commonly associated with coronary artery disease. In recent studies, annexin A1 gene (ANXA1) has been discovered to be involved in the treatment for MIRI. In this study, the primary focus was on the molecular mechanism of ANXA1 in polymorphonuclear neutrophil (PMN) infiltration and myeloperoxidase (MPO) activity in rats with MIRI. Initially, microarray analysis was carried out in order to identify differentially expressed genes. Moreover, a rat model of MIRI was established for evaluating the expression of ANXA1, signal transducer and activator of transcription 3 (STAT3) and vascular endothelial growth factor (VEGF) in myocardial tissues. Following this, the ANXA1 vector, siRNA-ANXA1, and Stattic (inhibitor of STAT3 signaling pathway) were utilized for analyzing the regulatory role of ANXA1 in physiological indexes, hemodynamic parameters, inflammatory factors, myocardial infarct size, MPO activity, PMN infiltration, and apoptosis of PMNs. Furthermore, the relationship between ANXA1 and STAT3 signaling pathway was analyzed. Initially, a reduction in the expression of ANXA1, STAT3 and VEGF in myocardial tissues of MIRI rats was found. To elaborate, overexpressed ANXA1 inhibited levels of inflammatory factors, the activation of PMN infiltration, reduced the degree of PMN infiltration, and decreased the apoptosis of PMNs. More importantly, down-regulated ANXA1 inhibited the activation of STAT3 signaling pathway, which thereby suppressed VEGF expression. With this all taken into account, the present study presents that up-regulated ANXA1 inhibits PMN infiltration and MPO activity by activation of STAT3 signaling pathway in rats with MIRI.

1. Introduction

Acute myocardial infarction (MI) and heart failure were acknowledged as the major causes of heart disease related death and the leading reasons of disability in the world [1]. Although timely reperfusion was the most effective therapeutic strategy for MI, reperfusion often coincided with cardiomyocyte death, *i.e.* myocardial ischemia-reperfusion injury (MIRI) [2]. As a complex pathophysiological event, MIRI is characterized by overload of $Ca2+$, accumulation of reactive oxygen species, induced inflammatory mediators, and interfered cellular ion homeostasis [3,4]. Multiple risk factors, which include hypertension, altered coronary circulation, heart failure, insulin resistance, diabetes, aging, as well as some clinical setting, such as thrombolytic therapy, coronary bypass surgery, and percutaneous transluminal coronary angioplasty have close connections with the occurrence and progression of MIRI [5,6]. Although progress has been made in attenuating MIRI,

Abbreviations: MIRI, Myocardial ischemia-reperfusion injury; ANXA1, annexin A1; PMN, polymorphonuclear neutrophil; MPO, myeloperoxidase; MI, myocardial infarction; GEO, Gene Expression Omnibus; NCBI, National Center for Biotechnology Information; IR, ischemia-reperfusion; GO, Gene Ontology; SPF, specific pathogen-free; SD, Sprague-Dawley; NC, negative control; *CF*, coronary flow; LVDP, left ventricular development pressure; HR, heart rate; HRP, horseradish peroxidase; SOD, superoxide dismutase; MDA, malondialdehyde; LDH, lactate dehydrogenase; ROS, reactive oxygen species; BSA, bovine serum albumin; HE, Hematoxylin-eosin

* Corresponding author at: Department of Cardiology, Beijing Anzhen Hospital, Capital Medical University, No. 2 Anzhen Road, Chaoyang District, Beijing 100029, PR China.
E-mail address: wuyongquan67@163.com (Y. Wu).

https://doi.org/10.1016/j.cellsig.2019.05.010
Received 28 February 2019; Received in revised form 21 May 2019; Accepted 22 May 2019
Available online 24 May 2019
0898-6568/

MIRI remains a major challenge in attaining effective therapy [7]. Thus, this calls for new and more accurate predictions and studies to help provide better therapeutic strategies of MIRI.

In addition, it has been discovered that several genes have functions on MIRI, such as pro-inflammatory cytokine genes (Toll-like receptor 4), and annexin A1 (ANXA1) [8,9]. As a member of the annexin superfamily of glucocorticoid-regulated proteins, ANXA1 is endowed with anti-inflammatory as well as pro-resolving properties [10]. As an illustration, a recent study has exploited that endogenous ANXA1 inhibited inflammatory cells infiltration into injured myocardium, enhanced myocardial viability, thereby attenuated MI [11]. Moreover, ANXA1 has played an important role in that it has been used for treating MIRI with good outcomes. ANXA1 has protective effects on MIRI by removing polymorphonuclear neutrophil (PMN) infiltration through macrophages and inhibiting inflammation in myocardial tissues [12]. Furthermore, previous study has reported that ANXA1 enhanced matrix metalloproteinase 2 by stimulating formyl peptide receptors through signal transducer and activation of transcription 3 (STAT3) and extracellular-signal-regulated kinase signaling pathways [13]. To elaborate, STAT3 is reported to be an effective mediator protein for cardio-protection [14]. It has been proven in a previous study that STAT3 signaling pathway was responsive to a number of cytokines and hormones and attenuated MIRI by inhibiting mitochondrial oxidative injury [15]. Hence, we speculate that ANXA1 may regulate MIRI through STAT3 signaling pathway.

Based on the aforementioned studies, the role of ANXA1 in the development and progression of MIRI is still in need of clarification. Therefore, a goal of this study is to generate a MIRI rat model to identify the possible molecular mechanism of ANXA1 and STAT3 signaling pathway underlying the disease.

2. Materials and methods

2.1. Ethics statement

In accordance with the Laboratory Animal Protection Provisions of Capital Medical University, all experimental animal feeding and experimental procedures were strictly carried out. All animal experiments in this study were used only by abiding with the Guiding Opinions on Treating Experimental Animals (Guo Ke Fa Cai Zi [2006] No. 398) issued by the Ministry of Science and Technology of the People's Republic of China, as well as the approval of the Guide for the Care and Use of Laboratory Animal issued by the National Institutes of Health (NIH Publication No. 85–23, revised 1996). The study was carefully conducted with the principles of completing experiments with the minimum number of animals and minimizing the suffering of experimental animals.

2.2. Microarray analysis

Gene Expression Omnibus (GEO) database was utilized for searching ischemia-reperfusion (IR) microarray data, and the GSE87023 microarray data was found. Then, the GSE87023 microarray data was downloaded for analysis which included three IR samples and six control samples. Selection of important differentially expressed genes was conduted through the use of empirical Bayes moderated *t*-statistics from the Bioconductor package limma in R language. Consequently, differentially expressed genes were annotated by the "annotate" package. A $p\ value < .05$ was considered statistically significant. Gene Ontology (GO) analysis of differential genes was performed using WEB-based GEne SeT AnaLysis Toolkit (http://www.webgestalt.org/).

2.3. MIRI model establishment

A total of 115 specific pathogen-free (SPF) grade male Sprague-Dawley (SD) rats (8 weeks old), with an average weight of 185 ± 10 g were purchased from Beijing Vital River Laboratory Animal Technology Co., Ltd. (Beijing, China). All rats were provided with adequate diet and drinking water. Rats were exposed to a fluorescent lamp every day and were contained in a quiet environment at a controlled room temperature of about 25 °C. A total of 100 rats were randomly gathered in order to establish rat models of MIRI. The success rate of the modeling was 90%, and the number of successful models was 90, which were then used as the IR group. Rats were anesthetized with ether, fixed, and the skin was incised longitudinally for a distance of 2 cm along the left sternal margin of the heart beating. The subcutaneous tissues and muscles were isolated by the layers with hemostatic forceps, and the left 2nd–4th ribs were exposed. The shadow of the pumping heart was clearly visible. The elbow hemostatic forceps were used to insert the ribs into the thoracic cavity along the 3–4 rib space of the left sternum to separate the ribs. The heart was popped out of the thoracic cavity, and the blood vessels were exposed. A 4/0 medical suture was used to thread the anterior descending branch of the coronary artery. Then, the heart was sent back to the thoracic cavity quickly. The ends of the medical suture were left for further use. Next, the skins and muscles of thoracic cavity and heart thread were clamped with long mouth hemostatic forceps to prevent pneumothorax. Following this set-up of the procedure, the changes in the electrocardiogram (ECG) were observed. The towering or inverted T wave was served as a marker of MI. If the change of ECG was not coherent, the hemostatic forceps should be slightly loosened and one end of the thread should be tightened. After this adjustment, the changes of ECG could be seen clearly. For reperfusion, the hemostatic forceps were loosened and the thread was loosened to form a MIRI model. Finally, at the end of the operation, the muscles, skin, and incision were sutured layer by layer. The incision was infused with penicillin and disinfected with iodophor to prevent any infection in the future. The remaining 15 rats were used as the sham group. Rats in the sham group went under the process of thoracotomy and only ligated the coronary artery without threading. Rats with one of the following conditions were excluded from the experiment: (1) failure of ligation of coronary artery or no reperfusion; (2) massive hemorrhage during ligation; (3) death caused by severe arrhythmia or pulmonary edema; (4) after being anesthetized by respiratory ether, the rats were fixated on the operating table in supine position, connected with ECG, monitored by limb leads, and recorded the ECG of lead II for 1 min at each time. Rats with abnormalities were excluded and disregarded [16].

2.4. Markers of successful establishment of MIRI rat model

After modeling, the ST-segment elevation or T-wave elevation or inversion with one-way curve of back-arch upward displayed in ECG were observed as the marker of MI. The success of the RI model was analyzed through the reduction of the elevated ST segment by > 50% or decreased towering T wave.

2.5. Animal treatments

Rats after successfully modeling were treated with ANXA1 negative control (NC) lentivirus vector, ANXA1 lentivirus vector, siRNA-ANXA1 lentivirus vector, Stattic (the STAT3 signaling pathway blocker, TargetMol, Boston, MA, USA), and ANXA1 vector + Stattic. SiRNA-ANXA1 lentiviral vectors were constructed according to Fang et al. [17]. In a brief explanation, the siRNA duplexes targeting ANXA1 (accession number, NM_000700) were designed online through the website of http://rnaidesigner.invitrogen. com/rnaiexpress/rnaiexpress.jsp. After annealing of synthetic Oligo DNA, the double-stranded DNA was ligated with the pGLV/H1/GFP vector digested by BamHI and *Eco*RI to form the pGLV-ANXA1-RNAi. Subsequently, PCR was carried out to screen positive clone, which was identified by sequencing. PGLV-ANXA1-RNAi and pGLV/helper-1, pGLV/helper-2, and pGLV/helper-3

were co-transfected into 293T cells to produce lentivirus particles LV-ANXA1-RNAi (siRNA-ANXA1), and the titer was determined. The ANXA1 gene was recognized and cloned into lentivirus plasmid PGC-Fu to construct ANXA1 vector. After the ANXA1 gene was digested and sequenced, the PGC-Fu-ANXA1 plasmid and packaging plasmids pHdper1.0 and pHelper2.0 were co-transfected into human embryonic adrenal epithelial cell line 293T cells. The recombinant lentivirus PGC-Fu-ANXA1 (ANXA1 vector) carrying ANXA1 gene and GFP gene was obtained with the titer determined.

The rats were anesthetized and then connected to the ventilator. Following this, the chest was opened. Next, 40 μL lentivirus vectors were injected into the outer layer of the myocardium through a multi-point injection to infect the myocardium of rats with a 50 μL micro-injector. The intercostal incision and skin incision were then quickly sutured.

2.6. Measurement of hemodynamic indexes

After treatment, all rats were cultured for approximately 24 h. Then, those rats after induction were anesthetized with 50 mg/kg phenobarbital intraperitoneally. After anesthesia, the pulmonary artery, common carotid artery, and tracheal intubation were linked with a four-channel physiological recording instrument. The hemodynamic parameters including coronary flow (*CF*), left ventricular development pressure (LVDP), maximum rate of pressure rise in the left ventricle (+dp/dtmax), heart rate (HR) were noted down.

2.7. Blood collection by cardiac puncture

Following the deeply anesthesia of rats, a 5 mL syringe with a 23G1 needle was inserted between at the location of the two ribs of the rat at a 45-degree angle. Whether there was blood in the needle should be noted since it may be indicative of successful insertion. A total of 3 mL blood was gently extracted and transferred into the tube. After a 3000 r/min centrifugation at a temperature of 4 °C for 10 min, the serum was collected and stored in a refrigerator at −20 °C [18].

2.8. Immunohistochemistry

Moreover, the rat myocardial tissue sections were obtained and baked at 60 °C for 1 h. Afterwards, sections were first dewaxed in three cylinders of xylene for 30 min (10 min per cylinder). Next, sections were dehydrated in 95%, 80%, and 75% gradient alcohols for 1 min, and then incubated with 3% H_2O_2 (84885, Sigma-Aldrich, San Francisco, CA, USA) for 30 min at 37 °C. After that, myocardial tissue sections were placed in a 0.01 M citrate buffer, boiled at 95 °C for 20 min, and then cooled down to room temperature. After being sealed with normal goat serum at 37 °C for 10 min, sections were probed with the primary antibody, rabbit anti-rat monoclonal antibody to ANXA1 (1: 4000, ab214486, Abcam Inc., Cambridge, MA, USA) overnight at 4 °C. Then sections were incubated with the secondary antibody, horseradish peroxidase (HRP)-labeled goat anti-rabbit antibody (DF7852, Shanghai Yaoyun Biotech Co., Ltd., Shanghai, China) for 30 min at room temperature to cool down. Sections were treated with streptomyces avidin-biotin-peroxidase complex for 30 min, stained with 3 mL diaminobenzidine (DAB; DA1010; Solarbio Science & Technology Co., Ltd., Beijing, China) for 5–10 min, counterstained with hematoxylin, and then finally sealed. According to the percentage of positive cells in at least five areas at high magnification, the staining of proteins was classified as followed; 1 for 5–25%; 2 representing 26–50%; 3 representing 51–75%; 4 representing > 75%. According to the staining intensity, the staining was assorted as followed: 1 for light yellow; 2 representing yellow or dark yellow; 3 brown or tan. Finally, the percentage of positive cells was calculated [19].

2.9. Detection of physiological indexes in myocardial tissues

In accordance with the instructions of the kit (No. ml001998, Shanghai Enzyme-Linked Biotechnology Co., Ltd., Shanghai, China), the superoxide dismutase (SOD) was detected. The detection of the activity of malondialdehyde (MDA) was performed according to the instructions of the kit (No. ml531021, Shanghai Enzyme-Linked Biotechnology Co., Ltd., Shanghai, China). The activity of SOD was determined by the xanthine oxidase method, and the MDA level was indirectly evaluated by the optical density (OD) value of the red product produced by the reaction of MDA with sodium thiobarbiturate. Serum lactate dehydrogenase (LDH) and creatinine phosphokinase isoenzyme (CK-MB) levels were evaluated with the use of an Olympus AU2700 automatic biochemical analyzer (Beckman Coulter, Tokyo, Japan).

2.10. Determination of granulocyte colony-stimulating factor (G-CSF) level

Following the instructions of rat G-CSF enzyme-linked immunosorbent assay (ELISA) kit (Shanghai Mingjin Biotech Co., Ltd., Shanghai, China), the G-CSF level in myocardial tissues of rat MIRI model was discovered by double antibody sandwich assay. In each rat model of MIRI, 3 mL whole serum of myocardial tissues was collected by a sterile dry syringe in the left ventricular artery. The purified rat G-CSF antibody was coated with a microplate to prepare a solid-phase antibody. A total of 10 μL serum of myocardial tissues (dilution: 5 times) was added into the microplate coated with monoclonal antibody, and then bound with HRP-labeled G-CSF antibody to form antibody-antigen-enzyme labeled antibody complex. The tissues were thoroughly washed and then the substrate 3,3′,5,5′-tetramethylbenzidine (TMB; EL0001, InnoReagents Co., Ltd., Huzhou, Zhejiang, China) was used for color development. TMB was converted to blue under the catalysis of HRP enzyme and converted to yellow color by the action of acid. The depth of color was positively correlated with G-CSF in the samples. The OD value was measured by a microplate reader at a wavelength of 450 nm, and the level of G-CSF in the serum of myocardial tissues was calculated according to the standard curve.

2.11. Detection of reactive oxygen species (ROS) level

Fifteen minutes after intraperitoneal injection of heparin 2000 U/kg, rats were euthanized. The thoracic cavity of rats was first cut with the use of scissors, and then the hemostatic forceps were used to expose the heart and the ascending aorta (aortic root). Following that, the pericardium was cut, and the heart was quickly cut off and washed in heparinized normal saline at a temperature of 4 °C. Then the aorta was intubated retrogradely, tightened with sutures, rapidly placed in a Langendorff perfusion system which was set to 36 °C–37 °C previously, and saturated with > 99% medical oxygen for > 30 min. During the whole perfusion period, the temperature was steady at 36–37 °C with saturated oxygen and oxygen flow rate of 0.3–0.5 L/min. The ventricles were isolated and sliced in a beaker containing 0.1% bovine serum albumin (BSA) calcium-free Tyrode solution with a scissor. At the same time, ventricles were triturated and then incubated at 36–37 °C for 5–10 min. The supernatant was diluted to about 25 mL using fresh calcium-free Tyrode solution containing 0.1% BSA. The ventricular tissue mass was triturated through the same method and were allowed to stand. In addition, the obtained cells were transferred into confocal dishes for the purpose of confocal microscopy. After cells had been adherent to the wells, the culture solution was decanted. Cells were stained with 400 μL 2′,7′-Dichlorodihydrofluorescein diacetate (DCFH-DA; 5 μmol/L), and water-bathed for 30 min at 37°. After being added with 400 μL the culture solution, the cells were measured [20].

2.12. Myeloperoxidase (MPO) activity assay

The content of PMNs in myocardial tissues could be carefully and quantitatively determined through the measurement of MPO activity of myocardial tissues in 6 rats. The MPO activity was detected by MPO activity assay, and then scanned spectrophotometrically at 460 nm for 2 min. The OD differences ($^{\Delta}$OD) between at 30th second and at 90th seconds were recorded. The change of OD within 1 min displayed the change in enzyme activity (*i.e.* the activity of one-unit MPO was defined as the amount of enzymes required to reduce peroxide by 1 μm per min at a temperature of 25 °C). The calculation formula for MPO activity (U/100 mg) = $^{\Delta}$OD/[11.3 × volume of myocardial tissues (mg/reaction solution)].

2.13. ELISA

After the process of successful induction, the inflammatory factors in the blood of myocardial tissues were detected with the use of ELISA kit (mll002859, Shanghai Enzyme-Linked Biotechnology Co., Ltd., Shanghai, China). Polyclonal antibodies to IL-6 (ab100772), IL-1β (ab100768), ICAM-1 (ab100763) and TNF-α (ab6671) were diluted to 1–10 μg/mL. All antibodies were purchased from Abcam Inc. (Cambridge, MA, USA). Furthermore, 0.1 mL antibody was added into each well for overnight incubation at a temperature of 4 °C. After that, 0.1 mL supernatant (× 2) was added into each well for a 1-h time interval for the purpose of incubation at 37 °C. The blank, negative and positive wells were prepared. Then, each well was added with 0.1 mL freshly diluted enzyme-labeled secondary antibody and incubated at 37 °C for about 35–60 min. Each well was stained with 0.1 mL freshly prepared TMB (EL0001, InnoReagents Co., Ltd., Huzhou, Zhejiang, China) at 37 °C for approximately 10–30 min. A total of 50 μL terminating solution was added to finalize the color development. Later, the OD value of each well was determined at the wavelength of 450 nm within 20 min [21].

2.14. 2,3,5-triphenyltetrazolium chloride (TTC) staining

After successful establishment of the rat model of MIRI, the atrium and right ventricles of rats were isolated and portioned into sections. The sections were immersed in 2% TTC phosphate buffer (pH = 7.4) at 37 °C and incubated for 30 min and then fixed with 10% formaldehyde solution for 24 h to enhance the color contrast. Following this treatment, the myocardial tissues were partitioned: light red representing the ischemic myocardium without infarction, and grayish white representing the infarcted myocardium. The infarct area was computed with the Motic microscopy image analysis software.

2.15. Hematoxylin-eosin (HE) staining

Sections of myocardial tissues were immersed in hematoxylin solution for 3–4 min, washed, and stained with eosin solution for 1–2 min. After the washing, the sections were dehydrated in 80%, 90% and 100% ethanol for 3–5 min, dewaxed with xylene for 3 min, and sealed with neutral gum. One portion from six rats in each group was taken, and five fields were randomly picked from each section. The number of PMNs was ciphered separately. The mean value was used as the representative value.

2.16. TdT-mediated dUTP-biotin nick end-labeling (TUNEL) staining

The TUNEL kit (Roche Diagnostics, Basel, Switzerland) was utilized for staining to observe the cell apoptosis of myocardial tissues. TUNEL reaction mixture was prepared according to TUNEL cell apoptosis detection kit. Cells were reacted with 50 μL TUNEL reaction solution (prepared with enzyme concentration solution and labeling solution at a ratio of 1: 9) for 50 min, and then incubated with 50 μL transformant-peroxidase (POD) at a high temperature of 37 °C for 30 min. Next, cells were developed with 3 mL DAB (DA1010, Solarbio Co., Ltd., Beijing, China) for 3 min, counterstained by hematoxylin for 3 s, and sealed with neutral gum. Five fields were randomly selected for the main purpose of observing. Following the observation, the percentage of positive cells in the total number of cells was calculated and served as the apoptotic rate. Apoptosis rate (AI) is represented as the number of apoptotic cells/total number of cells × 100% [22].

Table 1
Primer sequences for RT-qPCR.

Gene	Primer sequence
ANXA1	F: 5′-GCAGGCCTGGTTTATTGAAA-3′ R: 5′-GCTGTGCATTGTTTCGCTTA-3’
STAT3	F: 5′-CTAGACAATATCATCATCGACCTTG-3′ R: 5′-CCAAAGCCAGCACATAGG-3′
VEGF	F: 5′-CAGCCCTGGATCACAGTTTT-3′ R: 5′-TCTCCGCTCTCTGAACAAGG-3′
STAT5	F: 5′-GTAAACCATGGCTGTGTGGA-3′ R: 5′-AAATAATGCCGCACCTCAAT-3′
STAT6	F: 5′-CTCTGTGGGGCCTAATTTCCA-3′ R: 5′-CATCTGAACCGACCAGGAACT-3′
GAPDH	F: 5′-ATGGCACAGTCAAGGCTGAGA-3′ R: 5′-CGCTCCTGGAAGATGGTGAT-3′

Notes: RT-qPCR, reverse transcription quantitative polymerase chain reaction; ANXA1, annexin A1; STAT3, signal transducer and activator of transcription 3; VEGF, vascular endothelial growth factor; STAT5, signal transducer and activator of transcription 5; STAT6, signal transducer and activator of transcription 6; GAPDH, glyceraldehyde-3-phosphate dehydrogenase; F, forward; R, reverse.

2.17. RNA isolation and quantification

After transfection for 48 h, the total RNA was extracted with the miRNeasy Mini Kit (217004, QIAGEN, Duesseldorf, Germany). The primers of ANXA1, STAT3, and VEGF were designed and synthesized by Takara (Tokyo, Japan) (Table 1). In accordance with the instructions of PrimeScript RT kit (RR036A, Takara, Tokyo, Japan), the RNA was reversely recorded into complementary DNA (cDNA). The fluorescence quantitative PCR was conducted while following the instructions of a SYBR® Premix Ex TaqTM II kit (RR820A, TaKaRa, Tokyo, Japan) using an ABI 7500 quantitative PCR instrument (7500, ABI, Oyster Bay, N.Y., USA). With glyceraldehyde-3-phosphate dehydrogenase (GAPDH) gene playing the role as an internal reference, the fold changes were calculated by means of relative quantification ($^{2\text{-}\Delta\Delta Ct}$ method) [23].

2.18. Western blot analysis

Western blot analysis was performed according to the methods in previous literature [24]. The total amount of protein in tissues and cells was extricated using radio-immune precipitation assay lysis buffer (R0010, Solarbio Science & Technology Co, Ltd., Beijing, China) containing phenylmethanesulfonyl fluoride (PMSF). The obtained protein was separated by sodium dodecyl sulfate-polyacrylamide gel electrophoresis and was then transferred to a polyvinylidene fluoride membrane by the wet transfer method, and then blocked in 5% BSA at room temperature for 1 h. The membrane was probed with the primary antibody, rabbit anti-rat monoclonal antibodies to ANXA1 (1: 2000, ab214486), STAT3 (1: 1000, ab68153), STAT5 (1: 1000, ab16276), STAT6 (1: 1000, ab44718), and VEGF (1: 1000, ab32152) at 4 °C overnight. All the antibodies above were acquired from Abcam Inc. (Cambridge, MA, USA). Subsequently, HRP-conjugated goat anti-rabbit antibody to immunoglobulin G (IgG; 1: 5000; Beijing Zhongshan Biotech Co., Ltd., Beijing, China) was added on the membranes for the process of incubation. Additionally, the images of membranes were obtained after reaction with enhanced chemiluminescence solution

(WBKLS0500, Pierce Chemical Co., Rockford, IL, USA). The membranes were photographed using a Bio-Rad gel imaging analysis system (Bio-Rad, Hercules, CA, USA) and scrutinized using Quantity One software v4.6.2.

2.19. Statistical analysis

Data were analyzed with the use of the SPSS 21.0 software (IBM Corp. Armonk, NY, USA). Data were presented as mean ± standard deviation. Normal distribution and variance homogeneity test were performed. With normal distribution and homogeneity of the variance, the comparisons of data between two groups were carried out by unpaired *t*-test, and the comparisons among multiple groups were assessed by one-way analysis of variance. The results were considered statistically significant if the p value < .05.

3. Results

3.1. ANXA1 is lowly expressed in myocardial tissues of rats with MIRI and can regulate STAT3 signaling pathway

Initially, the gene expression datasets GSE87023 were attained from the GEO database. In the GSE87023 microarray data, a total of 1466 differentially expressed genes were screened. Through screening out candidate gene ANXA1 by microarray data analysis, the aim of this part of the procedure was to explore the molecular function and clinical significance of ANXA1 in MIRI. A previous study has reported that ANXA1 played a vital role in the treatment of cardiovascular diseases [25]. Furthermore, ANXA1 has the potential to work as a key mediator of the process of hypoxia-related metastasis in prostate cancer [26]. Moreover, it was demonstrated that ANXA1 played a role in a variety of cell types (PMNs, macrophages) and promoted inflammatory regression at multiple levels [27]. However, the exact function of ANXA1 in MIRI remains unclear. A heat map of differentially expressed genes in GSE87203 is illustrated in Fig. 1A. ANXA1 was discovered to be lowly expressed in rats with MIRI (Fig. 1B). Next, WEB-based GEne SeT AnaLysis Toolkit was used to generate a differential gene GO analysis map (Fig. 1C). The results indicated that the biological process (BP) was mainly enriched in the metabolic process, cellular component (CC) in membrane, and molecular function (MF) in protein binding. While taking the signaling pathway prediction site into consideration, we found that ANXA1 could regulate STAT3 signaling pathway [13,28]. These results imply that downregulated ANXA1 may be involved in MIRI through the STAT3 signaling pathway.

3.2. ANXA1, STAT3 and VEGF are lowly expressed in myocardial tissues of rats with MIRI

After the induction of rat MIRI models, the ECG of rats before and after induction revealed that the ST-segment elevation or T-wave elevation or inversion with one-way curve of back-arch upward displayed in ECG were observed as the marker of MI. The success of the RI model was marked by a reduction of the elevated ST segment by > 50% or decreased towering T wave (Fig. 2A). Immunohistochemistry was executed in order to examine the expression of ANXA1 in myocardial tissues. The results showed that after staining, light yellow to brownish yellow staining could be observed in the cytoplasm of myocardial tissues of sham-operated mice, which suggested the positive expression of ANXA1 (Fig. 2B). The expression of ANXA1 in MIRI rats (32.78% ± 7.11%) was significantly lower than that in sham-operated rats (79.60% ± 12.51%) (p < .05; Fig. 2C). In addition, the expressions of ANXA1, STAT3 and VEGF in myocardial tissues of rats were quantified by RT-qPCR and Western blot analysis. In comparison to the sham-operated rats, the results demonstrated that the mRNA expression of ANXA1, STAT3 and VEGF in MIRI rats were significantly lower (Fig. 2D). When compared to sham-operated rats, MIRI rats exhibited notably decreased protein expression levels of ANXA1, STAT3, VEGF, and the extent of STAT3 phosphorylation (Fig. 2E and F). All data suggested that the expression of ANXA1, STAT3 and VEGF in myocardial tissues of MIRI rats were down-regulated.

3.3. Up-regulated ANXA1 increases expression of CF, LVDP and +dp/dtmax, while decreases HR

In order to investigate the effects of ANXA1 on MIRI, the hemodynamic parameters were detected and recorded using the four-channels physiological recording instrument. When compared with the sham-operated rats, the detection of hemodynamic parameters (Fig. 3A–D) showed that the MIRI rats had significantly down-regulated levels of *CF*, LVDP and +dp/dtmax in the myocardial tissues and significantly up-regulated HR (all p < .05). Rats treated with siRNA-ANXA1 and Stattic showed remarkably decreased levels of *CF*, LVDP and +dp/dtmax and increased HR, while rats stimulated with ANXA1 vector had significantly induced levels of *CF*, LVDP and + dp/dtmax and dramatically reduced levels of HR (all p < .05). No remarkable statistical difference in hemodynamic parameters was observed among rats treated with NC and ANXA1 vector + Stattic and rats without treatment (p > .05). Taken together, the data suggested that up-regulation of ANXA1 increased expression of *CF*, LVDP and +dp/dtmax while it decreased HR expression levels through activating STAT3 signaling pathway, which thereby alleviates MIRI.

3.4. Up-regulated ANXA1 reduces myocardial infarct size

TTC staining was then employed to measure myocardial infarct size. In comparison with the sham-operated rats, the MIRI rats had significantly increased myocardial infarct sizes of myocardial tissues (p < .05). Rats stimulated with ANXA1 vector had significantly reduced myocardial infarct size of myocardial tissues, while rats treated with siRNA-ANXA1 or Stattic displayed significantly induced myocardial infarct sizes of myocardial tissues (both p < .05). When compared with the rats treated with NC and without treatment, no remarkable differences in myocardial infarct size of myocardial tissues were found in rats treated with both ANXA1 vector and Stattic. Regarding the myocardial infarct size of myocardial tissues, there was no significant difference between non-treated rats and rats treated with NC vector (p > .05) (Fig. 4A and B). This data suggested that up-regulation of ANXA1 reduced myocardial infarct size through the activation of STAT3 signaling pathway, thereby alleviating MIRI.

3.5. Up-regulated ANXA1 promotes myocardial SOD activity and lowers MDA level and serum LDH and CK-MB levels in rats

Following this, the physiological indexes in myocardial tissues were detected by ELISA (Fig. 5A–D). Compared with the sham-operated rats, the MIRI rats exhibited remarkably decreased SOD activity, increased MDA level, and serum levels of LDH and CK-MB (all p < .05). Rats treated with siRNA-ANXA1 or Stattic disclosed significantly reduced SOD activity, induced MDA level, and serum levels of LDH and CK-MB, while rats stimulated with ANXA1 vector showed opposite trends (all p < .05). Compared to those with non-treated rats and rats treated with NC vector, no notable statistical difference of the levels of physiological indexes was observed in rats treated with ANXA1 vector + Stattic. However, the levels of physiological indexes between non-treated rats and rats treated with NC exhibited no remarkable difference (p > .05). Collectively, these data indicated that up-regulation of ANXA1 contributed to activated activity of SOD and decreased MDA level in myocardial tissues, and inhibited LDH and CK-MB levels in serum of PMNs in rats.

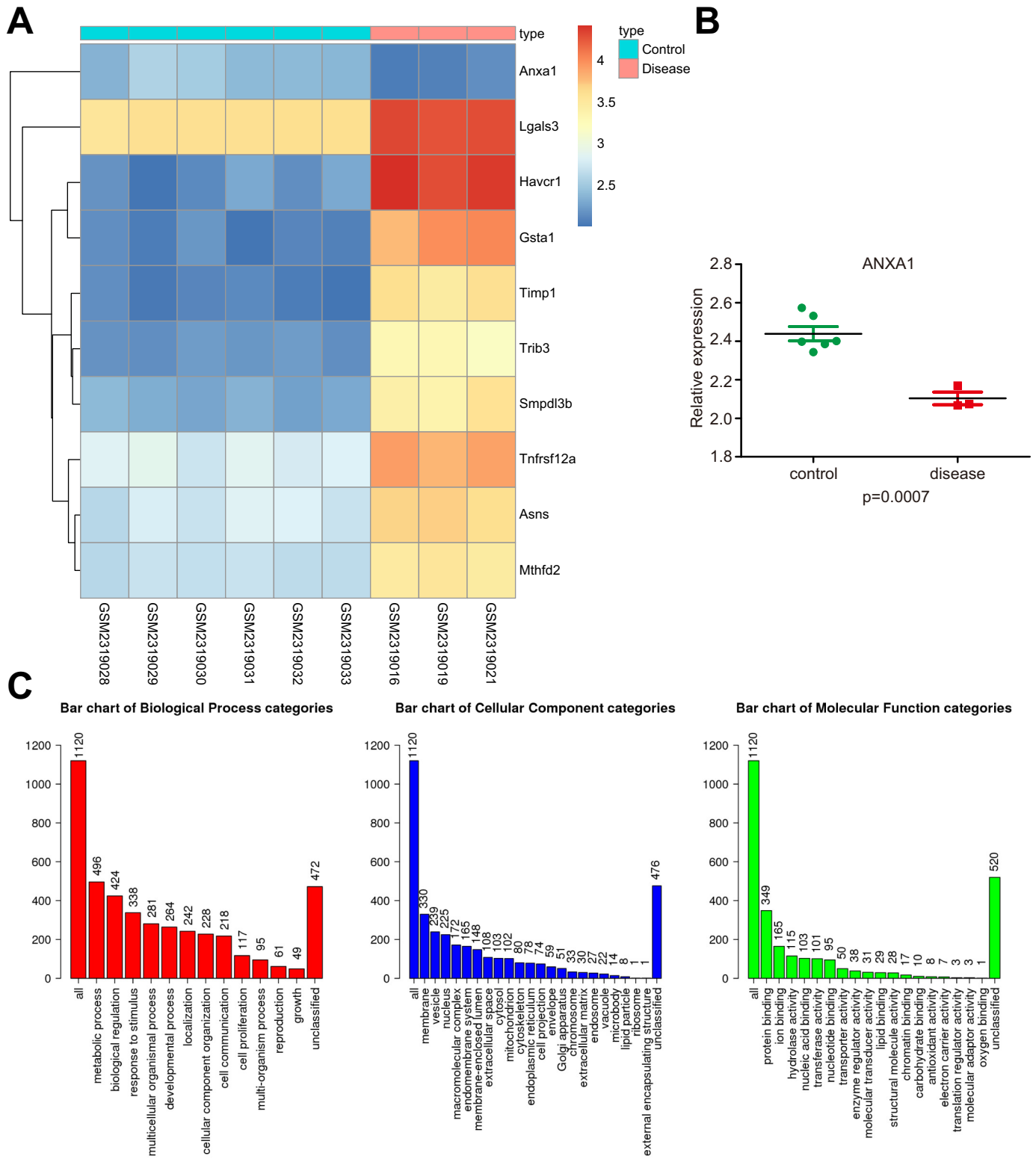

Fig. 1. ANXA1 and STAT3 signaling pathway are identified to be involved in MIRI. (A) the heatmap of differentially expressed genes in GSE87203. The abscissa represented the sample number, the ordinate represented the gene name, the upper tree represented the cluster of sample types, and the right chromatic histogram represented the gene expression level. Red represented high expression, green represented low expression. Each box in the graph represented the expression of a gene in one sample. The left dendrogram represented the clustering of gene expression. (B) the expression of ANXA1 in rats with MIRI and sham-operated rats was analyzed by microarray analysis. Green represented the sham-operated rats, and the red represented the MIRI rats. $p < .0001$ *vs.* the sham-operated rats. C, the GO analysis of differential expressed genes was analyzed by http://www.webgestalt.org/. (For interpretation of the references to color in this figure legend, the reader is referred to the web version of this article.)

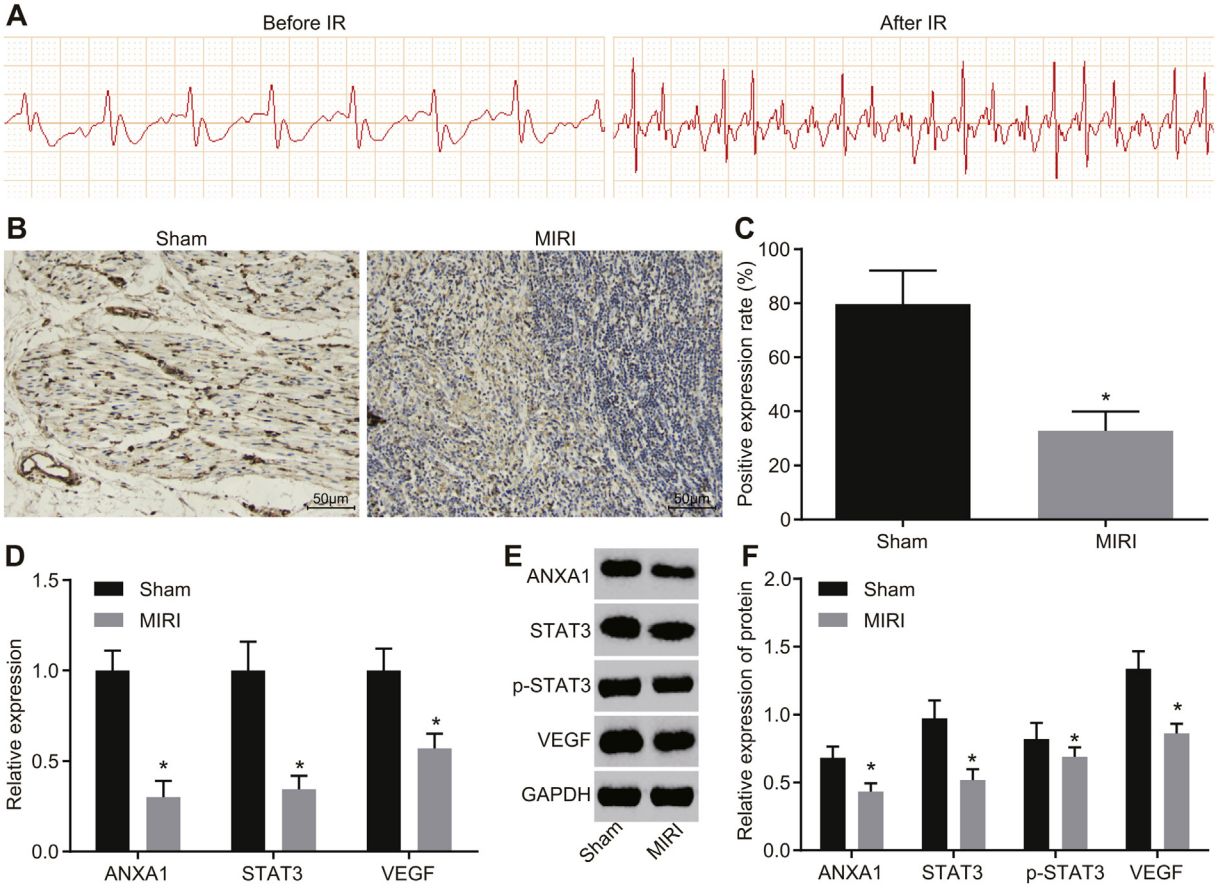

Fig. 2. The expression of ANXA1, STAT3 and VEGF in myocardial tissues of MIRI rats are decreased. Rats were either induced with MIRI or sham-operated. (A) ECG before and after the successful induction of IR model in rats. (B) the immunohistochemical staining of ANXA1 in myocardial tissues of MIRI rats and sham-operated rats (200 ×, 25 μm). (C) the statistical analysis of panel (B). (D) the mRNA expression of ANXA1, STAT3 and VEGF in MIRI rats and sham-operated rats determined by RT-qPCR. *E*-F, the protein expression of ANXA1, STAT3, VEGF, and the extent of STAT3 phosphorylation in MIRI rats and sham-operated rats examined by western blot analysis. $^{*}p < .05$ *vs.* the sham-operated rats. The results were measurement data, which were expressed as mean ± standard deviation. $n = 6$. Comparisons between two groups were conducted by independent *t*-test. All the experiments were repeated 3 times independently.

3.6. Up-regulated ANXA1 promotes release of G-CSF and inhibits the content of ROS in myocardial tissues

Afterwards, the G-CSF and ROS contents in myocardial tissues of MIRI rats were determined using double antibody sandwich assay and DCFH-DA method, respectively. The results showed that compared with the sham-operated rats, the MIRI rats had significantly decreased G-CSF content but increased content of ROS in the serum of myocardial tissues ($p < .05$). Rats treated with siRNA-ANXA1 or Stattic indicated remarkably reduced G-CSF content and induced ROS content in the serum of myocardial tissues, while rats stimulated with ANXA1 vector exhibited an opposite result ($p < .05$). When compared with the non-treated rats and rats treated with NC vector, no remarkable difference was shown in the G-CSF and ROS contents in myocardial tissues was observed in rats treated with ANXA1 vector + Stattic, and the G-CSF and ROS contents in myocardial tissues between non-treated rats and rats treated with NC vector had no statistical meaning ($p > .05$; Fig. 6A and B). These results revealed that up-regulation of ANXA1 promoted the release of G-CSF from PMNs into serum and inhibited ROS content in cardiomyocytes. Furthermore, the inhibition of STAT3 signaling pathway constrained the release of G-CSF from PMNs into serum and promoted ROS content in cardiomyocytes.

3.7. Up-regulated ANXA1 inhibits the expression of inflammatory factors in blood

Moreover, the effects of ANXA1 on the inflammatory factors were measured with the use of ELISA. The results (Fig. 7A–D) implied that compared with the sham-operated rats, the MIRI rats exhibited significantly potentiated serum levels of IL-6, IL-1β, ICAM-1, and TNF-α in the myocardial tissues (all $p < .05$). The serum levels of IL-6, IL-1β, ICAM-1, and TNF-α in myocardial tissues was remarkably up-regulated in rats treated with siRNA-ANXA1 or Stattic, while profoundly down-regulated in rats stimulated with ANXA1 vector (all $p < .05$). Therefore, no remarkable difference in the serum levels of IL-6, IL-1β, ICAM-1, and TNF-α in the myocardial tissues was observed in rats treated with ANXA1 vector + Stattic when compared with non-treated rats and rats treated with NC ($p > .05$). All this data advocated the fact that the up-regulation of ANXA1 decreased the levels of IL-6, IL-1β, ICAM-1, and TNF-α in the serum of myocardial tissues.

3.8. Up-regulated ANXA1 reduces PMN infiltration by activating STAT3 signaling pathway

The activity of MPO is closely related to the content of PMNs in myocardial tissues, so the activity of MPO could be used as an indicator of PMNs aggregation in myocardial tissues. The results discovered that compared with the sham-operated rats, the MIRI rats had significantly increased MPO activity in myocardial tissues (all $p < .05$). Rats stimulated with ANXA1 vector had notably diminished MPO activity in myocardial tissues, while rats treated with siRNA-ANXA1 or Stattic exhibited increased MPO activity in myocardial tissues (all $p < .05$). No significant difference was observed in rats treated with ANXA1 vector + Stattic when compared with non-treated rats and rats treated

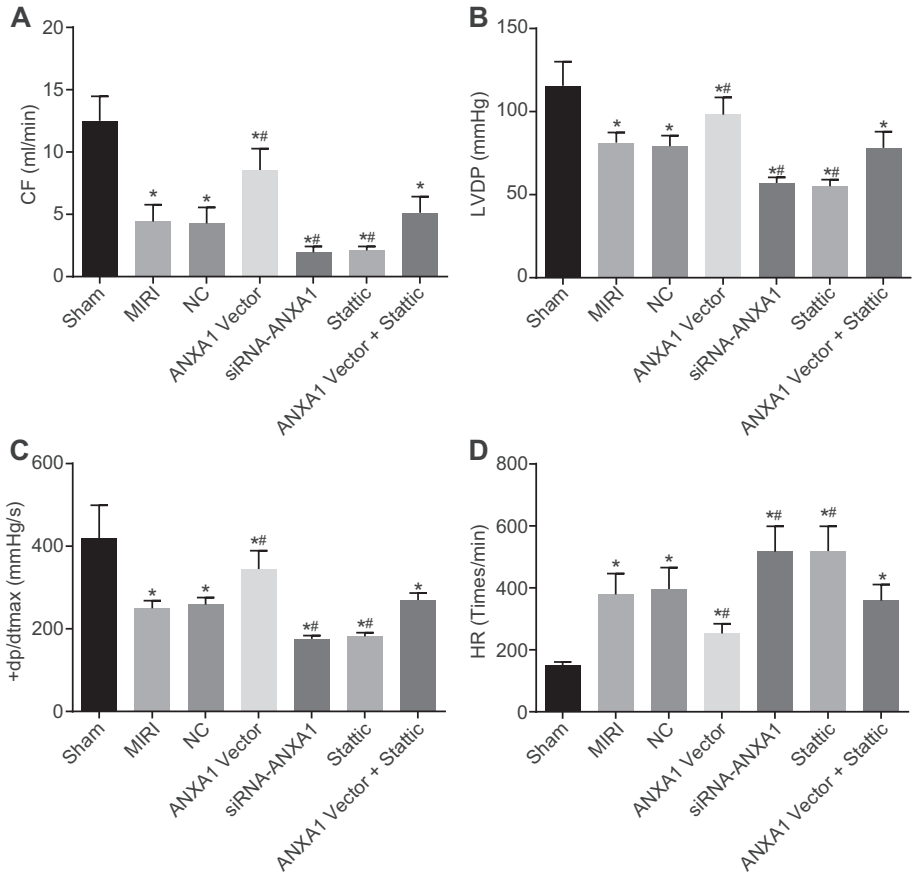

Fig. 3. Overexpressed ANXA1 promotes the level of *CF*, LVDP and +dp/dtmax, and inhibits HR. MIRI rats were treated with siRNA-ANXA1, ANXA1 vector and/or Stattic. (A) level of *CF* of rats. (B) level of LVDP of rats. (C) level of + dp/dtmax of rats. (D) level of HR of rats. $^{*}p < .05$ *vs.* the sham-operated rats. $^{\#}p < .05$ *vs.* the MIRI rats without treatment or treated with NC. $n = 6$. The results were measurement data, which were expressed as mean ± standard deviation. Comparisons among multiple groups were assessed by one-way analysis of variance. All the experiments were repeated 3 times independently.

with NC ($p > .05$). The MPO activity between non-treated rats and rats treated with NC vector exhibited no remarkable difference ($p > .05$; Fig. 8A).

Subsequently, HE staining was adopted to detect PMNs infiltration in myocardial tissues of rats. The myocardial fibers of sham-operated rats were observed to arrange neatly, the boundary of myocardial tissues was intact, and the myocardial transverse stripes were clear. However, the myocardial transverse stripes were lost while a large number of myocardial necrosis accompanied by PMN infiltration occurred in MIRI rats (Fig. 8B). The MIRI rats had significantly increased number of PMN infiltration when compared to sham-operated rats ($p < .05$). Rats stimulated with ANXA1 vector had notably reduced number of PMN infiltration in myocardial tissues, while rats treated with siRNA-ANXA1 or Stattic showed remarkably increased amounts of PMN infiltration in myocardial tissues ($p < .05$). Additionally, no evident difference was evaluated in rats treated with ANXA1 vector + Stattic when compared with non-treated rats and rats treated with NC ($p > .05$). The number of PMN infiltration between

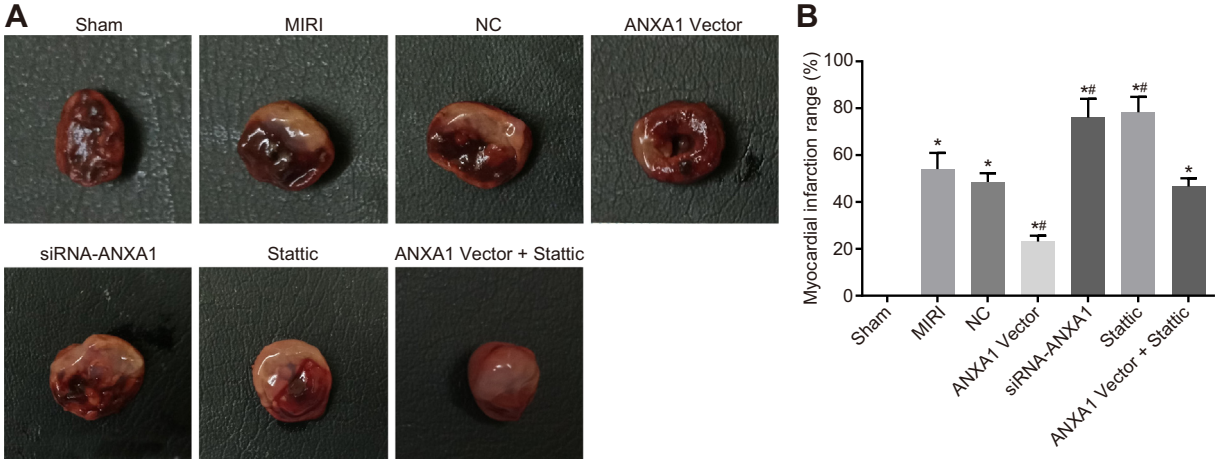

Fig. 4. Overexpressed ANXA1 reduces myocardial infarct size by activating STAT3 signaling pathway. MIRI rats were treated with siRNA-ANXA1, ANXA1 vector and/or Stattic. (A) representative images of the myocardial infarct size analyzed by TTC staining. (B) the statistical analysis of myocardial infarct size. $^{*}p < .05$ *vs.* the sham-operated rats. $^{\#}p < .05$ *vs.* the MIRI rats without treatment or treated with NC. $n = 4$. The results were measurement data, which were expressed as mean ± standard deviation. Comparisons among multiple groups were assessed by one-way analysis of variance. All the experiments were repeated 3 times independently.

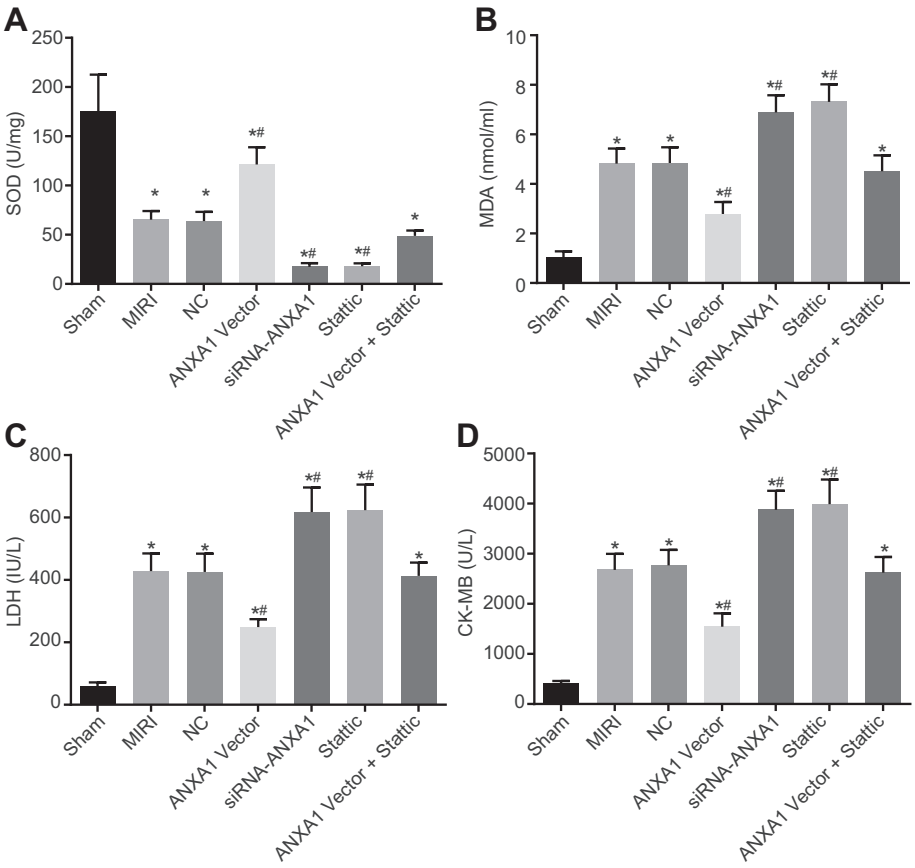

Fig. 5. Overexpressed ANXA1 inhibits the levels of MDA, LDH, CK-MB, while restores the SOD activity. MIRI rats were treated with siRNA-ANXA1, ANXA1 vector and/or Stattic. (A) the activity of SOD detected by xanthine oxidase method. (B) MDA level was indirectly evaluated by the OD value of the red product produced by the reaction of MDA with sodium thiobarbiturate. (C) the LDH level determined using an Olympus AU2700 automatic biochemical analyzer. (D) the CK-MB level determined using an Olympus AU2700 automatic biochemical analyzer. $^{*}p < .05$ *vs.* the sham-operated rats. $^{\#}p < .05$ *vs.* the MIRI rats without treatment or treated with NC. The results were measurement data, which were expressed as mean ± standard deviation. $n = 6$. Comparisons among multiple groups were assessed by one-way analysis of variance. All the experiments were repeated 3 times independently. (For interpretation of the references to color in this figure legend, the reader is referred to the web version of this article.)

non-treated rats and rats treated with NC had no statistical difference ($p > .05$; Fig. 8C). Thus, up-regulation of ANXA1 suppressed MPO activity and PMN infiltration *via* activating STAT3 signaling pathway in myocardial tissues.

3.9. Up-regulated ANXA1 reduces apoptosis of PMNs

TUNEL staining was used to detect cell apoptosis. As illustrated in Fig. 9A and B, the positive nuclei appeared as brown and the normal nuclei appeared as light blue. Compared with the sham-operated rats, the MIRI rats had significantly increased apoptosis of PMNs in myocardial tissues ($p < .05$). The apoptosis of PMNs in myocardial tissues was notably lower in rats stimulated with ANXA1 vector, while it was profoundly higher in rats treated with siRNA-ANXA1 or Stattic ($p < .05$). When compared with the non-treated rats and rats treated with NC, no significant difference in the apoptosis of PMNs in myocardial tissues was witnessed in rats treated with ANXA1 vector + Stattic, and the apoptosis of PMNs in myocardial tissues between non-treated rats and rats treated with NC had no statistical meaning ($p > .05$). All data proposed that the up-regulation of ANXA1 inhibited apoptosis of PMNs in myocardial tissues of MIRI rats.

3.10. Down-regulated ANXA1 inhibits the activation of the STAT3 signaling pathway

Finally, in order to figure out the relation between ANXA1 and STAT3 signaling pathway, the expression levels of ANXA1, STAT3, VEGF, and the extent of STAT3 phosphorylation were measured using PR-qPCR and western blot analysis. Rats stimulated with ANXA1 vector had notably increased expressions of ANXA1, STAT3, VEGF, and the

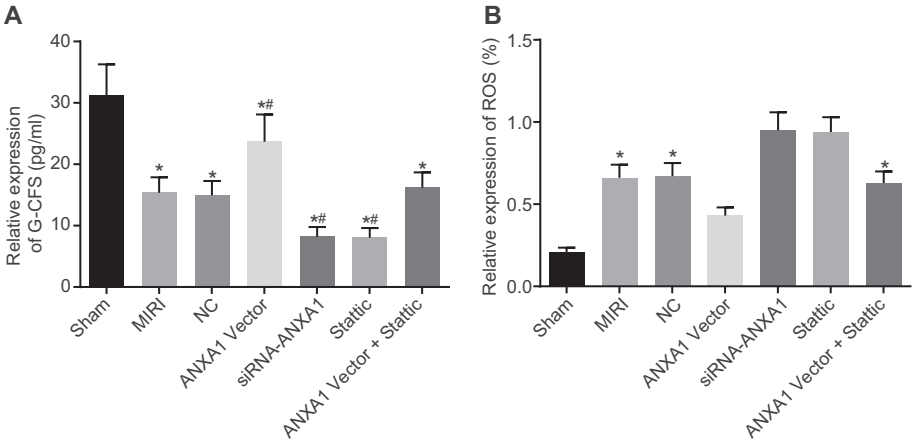

Fig. 6. Overexpressed ANXA1 enhances the release of G-CSF from PMNs into serum and suppresses ROS content in cardiomyocytes. MIRI rats were treated with siRNA-ANXA1, ANXA1 vector and/or Stattic. (A) the G-CSF content in myocardial tissues determined by double antibody sandwich assay. (B) ROS content in myocardial tissues determined by DCFH-DA method. $^{*}p < .05$ *vs.* the sham-operated rats. $^{\#}p < .05$ *vs.* the MIRI rats without treatment or treated with NC. The results were measurement data, which were expressed as mean ± standard deviation. Comparisons among multiple groups were assessed by one-way analysis of variance. $n = 6$. All the experiments were repeated 3 times independently.

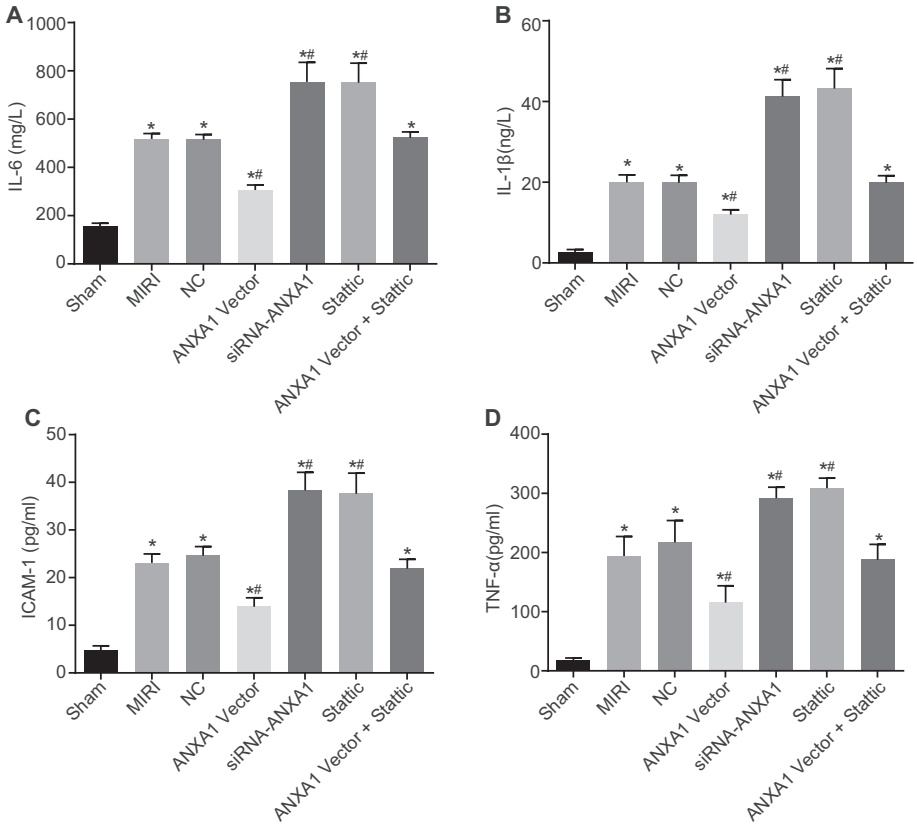

Fig. 7. Overexpressed ANXA1 inhibits the serum levels of inflammatory factors (IL-6, IL-1β, ICAM-1, and TNF-α). MIRI rats were treated with siRNA-ANXA1, ANXA1 vector and/or Stattic. (A) the serum levels of IL-6 in the myocardial tissues determined by ELISA. (B) the serum levels of IL-1β in the myocardial tissues determined by ELISA. (C) the serum levels of ICAM-1 in the myocardial tissues determined by ELISA. (D) the serum levels of TNF-α in the myocardial tissues determined by ELISA. $^{*}p < .05$ *vs.* the sham-operated rats. $^{\#}p < .05$ *vs.* the MIRI rats without treatment or treated with NC. The results were measurement data, which were expressed as mean ± standard deviation. $n = 6$. Comparisons among multiple groups were assessed by one-way analysis of variance. All the experiments were repeated 3 times independently.

extent of STAT3 phosphorylation, while rats treated with siRNA-ANXA1 or Stattic exhibited decreased expressions of ANXA1, STAT3, VEGF, and the extent of STAT3 phosphorylation (all $p < .05$). No significant difference was observed in rats treated with ANXA1 vector + Stattic when compared with the non-treated rats and rats treated with NC ($p > .05$). The expression of ANXA1, STAT3, VEGF, and the extent of STAT3 phosphorylation between non-treated rats and rats treated with NC exhibited no remarkable difference (all $p > .05$; Fig. 10A–C). Meanwhile, the expression of STAT5 and STAT6 was calculated and quantified by RT-qPCR and western blot analysis as well. The results showed that there was no important difference in protein and mRNA expression of STAT5 and STAT6 after ANXA1 vector or siRNA-ANXA1 treatments *versus* IR rats without treatment and those treated with NC. Besides, no significant difference was found in between rats treated with ANXA1 vector and siRNA-ANXA1 neither (all $p > .05$; Fig. 10D–F). These data suggested that down-regulation of ANXA1 inhibited STAT3 signaling pathway without exerting any roles in the expression of other proteins (STAT5 and STAT6) in the STAT family, thereby reducing VEGF expression in myocardial tissues.

4. Discussion

The incidence of MIRI has experienced rapid increases worldwide, and this disease is recognized as one of the main causes of morbidity and mortality in terms of heart disease around the world [29]. Despite the minimal amount of knowledge that has been uncovered, the molecular mechanisms of MIRI are not fully elucidated. Recent research have revealed that some signaling pathways could work as key mediators among pathogenic and pathological progression of MI controlled by related genes [30]. Through the establishment of a MIRI model in rats, the current study exploited the potential roles of ANXA1 and STAT3 signaling pathway in PMNs infiltration and MPO activity, and reached the conclusion that up-regulation of ANXA1 induced the activation of STAT3 signaling pathway and effectively inhibited PMNs infiltration and MPO activity in MIRI rats.

At first, low expression levels of ANXA1, STAT3 and VEGF were found in myocardial tissues of MIRI rats. Consistent with our study, Qin et al. also demonstrated that ANXA1 was down-regulated in MIRI and up-regulated ANXA1 could inhibit neutrophil infiltration and preserve the viability of cardiomyocyte [12]. Furthermore, down-regulated STAT3 expression that is correlated with induced myocardial infarct size was found in streptozotocin-induced diabetic rats with MIRI [31]. Additionally, previous study demonstrated that cell protective growth factors including VEGF contributed to MIR protection [32]. Up-regulated VEGF was revealed to induce cerebral blood flow and inhibit neurological injury after experimental ischemic brain damage [33].

Moreover, this study found that overexpressed ANXA1 attenuated MIRI, as supported by increased *CF*, LVDP and + dp/dtmax, G-CSF levels, decreased HR, levels of inflammatory factors and ROS, and reduced myocardial infarct size. It was described that decreased cardiac hemodynamic parameters (*CF*, LVDP and +dp/dtmax, G-CSF) and reduced infarct size were found in patients suffering from cardiac I/R injury [34]. IRI of the lower extremities was closely realted to the elevated release of proinflammatory cytokines from neutrophils including IL-6 and TGF-α [35]. Interestingly, up-regulated ROS was proved to be one of the major reasons for MIRI [36]. Up-regulated ANXA1 was involved in decreasing levels of ROS and inhibiting proinflammatory responses in PC12 cells [37]. In the brain, ANXA1 which acts as an endogenous protein, showed strong anti-inflammatory characteristics and was found to regulate inflammatory responses [38,39]. Additionally, ANXA1 has protective effects on MIRI by suppressing inflammatory cells infiltration into injured myocardium, enhancing myocardial viability, and attenuating MI [11].

Finally, it was proved that STAT3 signaling pathway was positively regulated by ANXA1 in this study. It is known that ANXA1 was an upstream regulator that controls several signaling pathway. For example, up-regulation of ANXA1 suppressed activation of inflammatory monocyte through formyl peptide receptors *via* JAK/STAT/suppressor

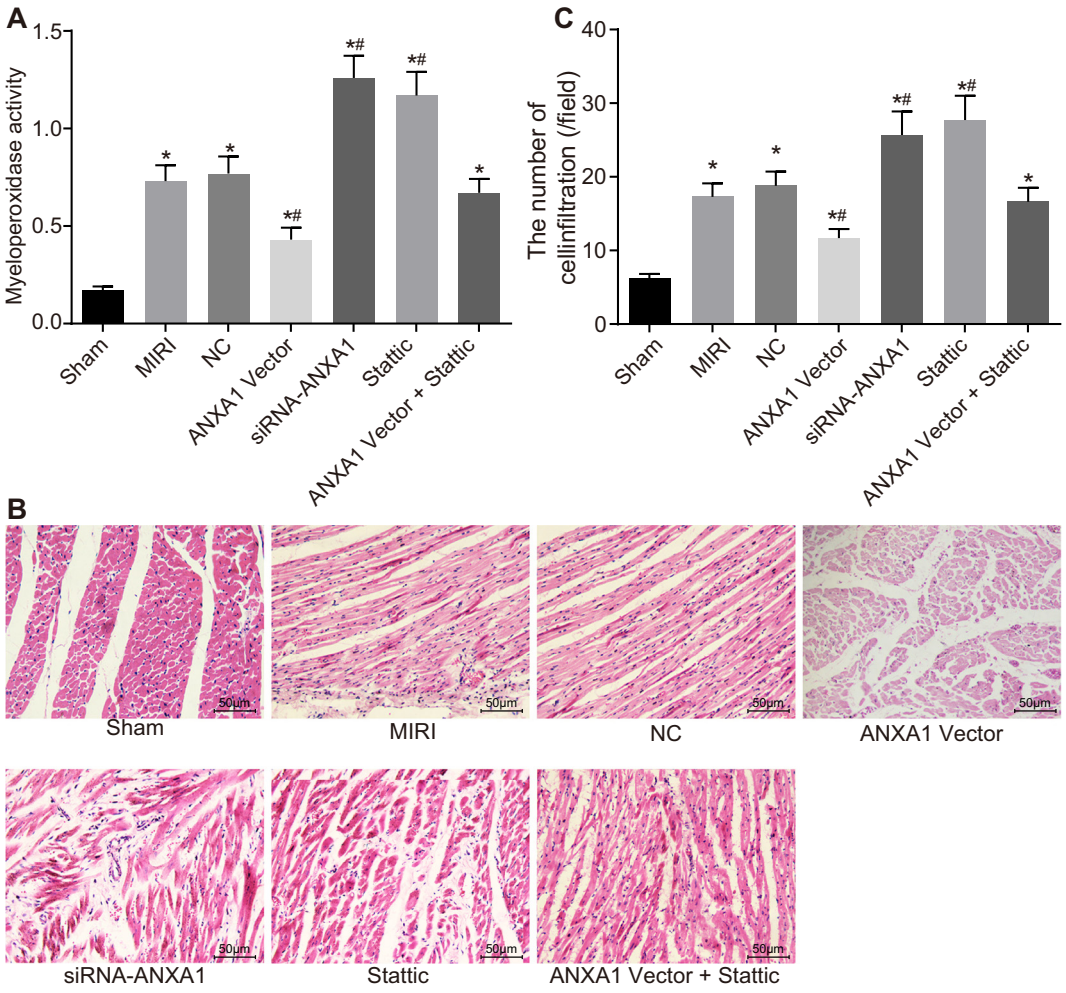

Fig. 8. Overexpressed ANXA1 inhibits MPO activity and PMN infiltration through the activation of STAT3 signaling pathway. MIRI rats were treated with siRNA-ANXA1, ANXA1 vector and/or Stattic. (A) the MPO activity in myocardial tissues examined by MPO activity assay. (B) HE staining of PMN infiltration. C, the number of PMN infiltration. $n = 6$. $^{*}p < .05$ *vs.* the sham-operated rats. $^{\#}p < .05$ *vs.* the MIRI rats without treatment or treated with NC. The results were measurement data, which were expressed as mean ± standard deviation. Comparisons among multiple groups were assessed by one-way analysis of variance. All the experiments were repeated 3 times independently.

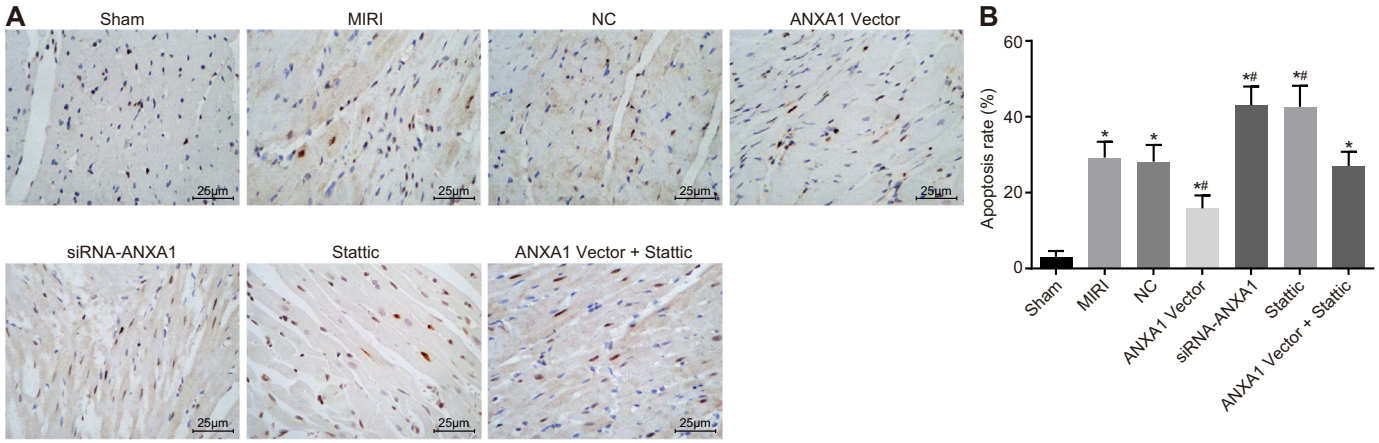

Fig. 9. Overexpressed ANXA1 suppresses apoptosis of PMNs in myocardial tissues. MIRI rats were treated with siRNA-ANXA1, ANXA1 vector and/or Stattic. (A) TUNEL staining of PMNs in myocardial tissues (400 ×; 25 μm). (B) the AI of PMNs in myocardial tissues. $^{*}p < .05$ *vs.* the sham-operated rats. $^{\#}p < .05$ *vs.* the MIRI rats without treatment or treated with NC. The results were measurement data, which were expressed as mean ± standard deviation. $n = 6$. Comparisons among multiple groups were assessed by one-way analysis of variance. All the experiments were repeated 3 times independently.

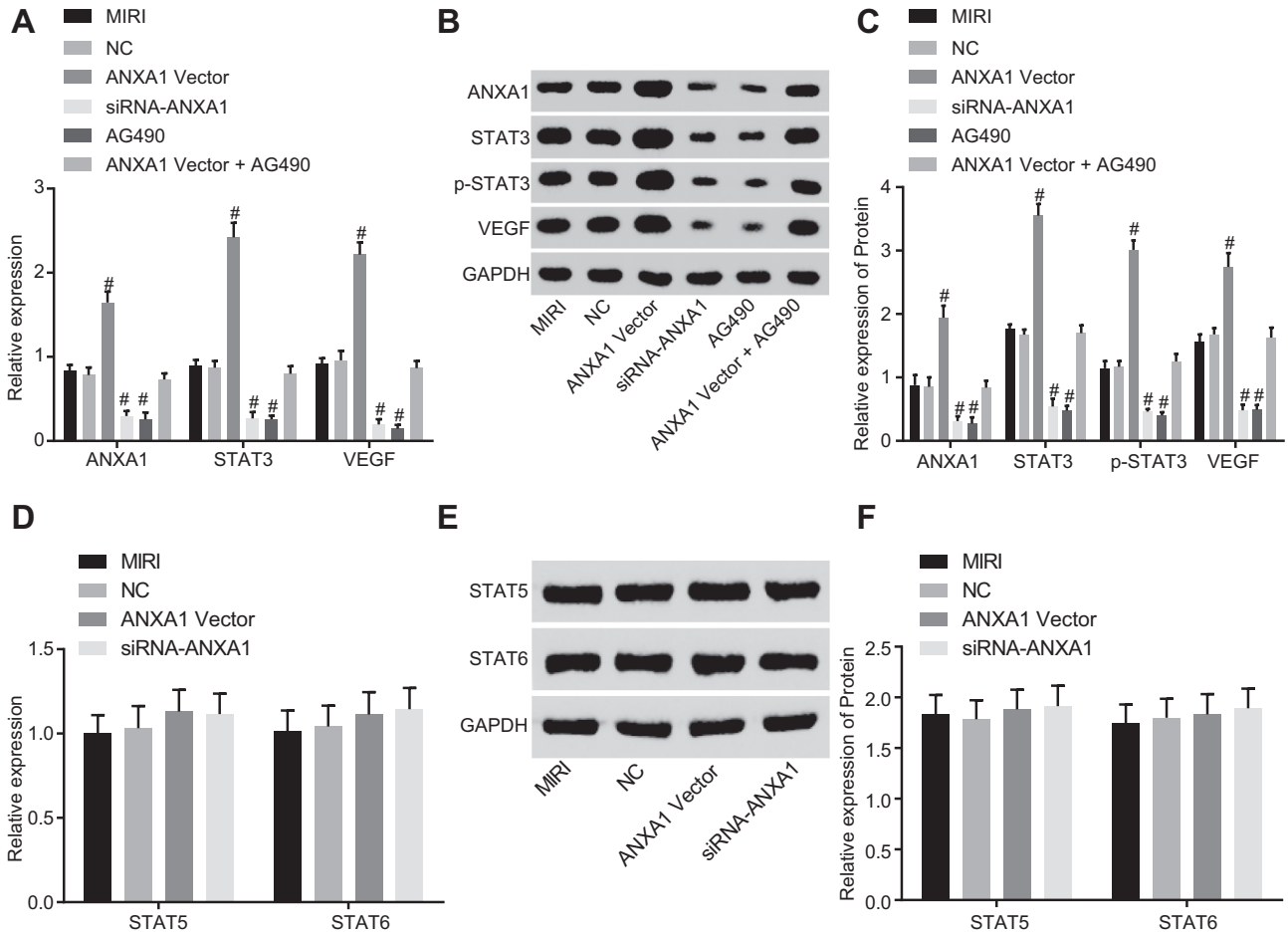

Fig. 10. Down-regulated ANXA1 blocks the STAT3 signaling pathway in myocardial tissues. MIRI rats were treated with siRNA-ANXA1, ANXA1 vector and/or Stattic. (A) the mRNA expression of ANXA1, STAT3, and VEGF in myocardial tissues determined using RT-qPCR. (B—C) the protein expression of ANXA1, STAT3, VEGF, and the extent of STAT3 phosphorylation in myocardial tissues measured by western blot analysis. (D) the mRNA expression of STAT5 and STAT6 in myocardial tissues determined using RT-qPCR. *E*-F, the protein expression of STAT5 and STAT6 in myocardial tissues measured by western blot analysis. $^{\#}p < .05$ *vs.* the sham-operated rats. $^{\#}p < .05$ *vs.* the MIRI rats without treatment or treated with NC. The results were measurement data, which were expressed as mean ± standard deviation. Comparisons among multiple groups were assessed by one-way analysis of variance. All the experiments were repeated 3 times independently; $n = 6$.

of cytokine signaling 3 signaling pathway [40]. Matrix metalloproteinase-2-ANXA1 induction was achieved by mitogen-activated protein kinase (MAPK) and STAT3 signaling pathways [13]. Furthermore, this study demonstrated that overexpressed ANXA1 inhibited PMNs infiltration and MPO activity of myocardial tissues but accelerated neutrophil apoptosis in MIRI by activating STAT3 signaling pathway. Torres et al. asserted that ANXA1, an endogenous anti-inflammatory protein, participated in the reduction of neutrophil-endothelial interactions as well as the acceleration of neutrophil apoptosis [41]. Another study established that induced ANXA1 and its mimetic counterparts had the ability to suppress accumulation of neutrophils through reduction of leukocyte infiltration and activation of neutrophil apoptosis [42]. In addition, Janus Kinase 2/STAT3 signaling pathway together with rapamycin was involved in protecting against MIRI by reducing infarct size, improving cardiac function following ischemia–reperfusion, and inhibiting cardiomyocyte apoptosis [43]. Moreover, some chemicals were determined to regulate infiltration and inflammation through STAT3 signaling pathway. For instance, Kim et al. demonstrated that 1-palmitoyl-2-linoleoyl-3-acetyl-rac-glycerol (PLAG) declined the migration of differentiated PMNs, and suppressed PMN infiltration, thereby ameliorating arthritic joints by activating IL-6/STAT3 signaling pathway [44]. It was then reported that sodium propionate was incorporated in the inhibition of the inflammation and reduction in MPO activity in dextran sulfate sodium-induced colitis mice by activating STAT3 signaling pathway [45]. Collectively, this study suggested that ANXA1 may be an important target for MIRI treatment, which regulated the pathogenesis of MIRI by regulating STAT3 signaling pathway.

Until recently, studies on the cardioprotective effects of ANXA1 and its peptidomimetics (Ac2–26, CGEN-855A) focused mainly on its anti-inflammatory effects as a mechanism for maintaining myocardial viability after IR injury [9,12]. This present study provides a new molecular mechanism for the direct protection of myocardial tissues by ANXA1. In summary, the data could serve as an explanation that overexpression of ANXA1 could inhibit PMNs infiltration and MPO activity of myocardial tissues in rat model of MIRI by activating STAT3 signaling pathway (Fig. 11B). Investigation on the functions of ANXA1 in MIRI and their functions may have potentially important therapeutic implications in the treatment of PMNs infiltration and MPO activity in MIRI. Although these findings may have a significant implication for the development of MIRI, the mechanism mediating the interaction between ANXA1 and STAT3 signaling pathway on MIRI still remains unclear and is in need of more investigation.

Acknowledgments

We would like to thank our researchers for their hard work and reviewers for their valuable advice.

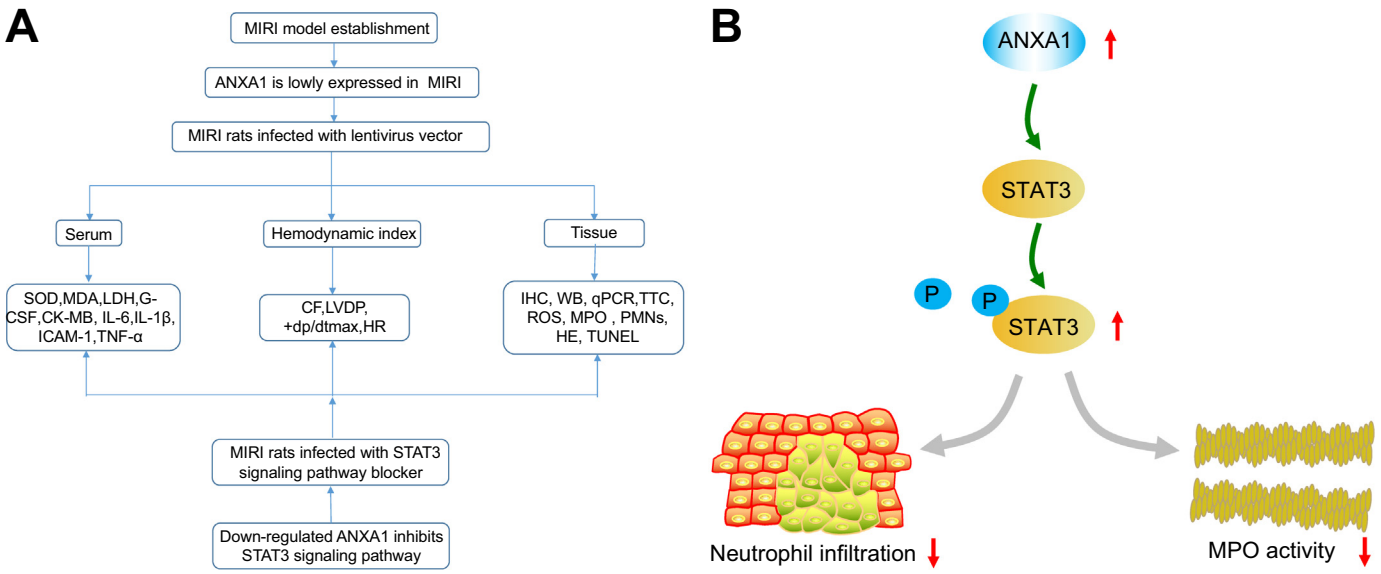

Fig. 11. The experimental flow chart and the mechanism diagram concerning the ANXA1 in MIRI. (A) the experimental flow chart. (B) Up-regulation of ANXA1 activated STAT3 signaling pathway, thereby inhibiting PMN infiltration and MPO activity in MIRI rats.

Funding

None.

Conflict of interest

None.

References

[1] S.B. Ong, S. Hernandez-Resendiz, G.E. Crespo-Avilan, R.T. Mukhametshina, X.Y. Kwek, H.A. Cabrera-Fuentes, D.J. Hausenloy, Inflammation following acute myocardial infarction: multiple players, dynamic roles, and novel therapeutic opportunities, Pharmacol. Ther. 186 (2018) 73–87.
[2] D.J. Hausenloy, D.M. Yellon, Myocardial ischemia-reperfusion injury: a neglected therapeutic target, J. Clin. Invest. 123 (1) (2013) 92–100.
[3] A.V. Zima, L.A. Blatter, Redox regulation of cardiac calcium channels and transporters, Cardiovasc. Res. 71 (2) (2006) 310–321.
[4] L. Minutoli, D. Puzzolo, M. Rinaldi, N. Irrera, H. Marini, V. Arcoraci, A. Bitto, G. Crea, A. Pisani, F. Squadrito, V. Trichilo, D. Bruschetta, A. Micali, D. Altavilla, ROS-mediated NLRP3 inflammasome activation in brain, heart, kidney, and testis ischemia/reperfusion injury, Oxidative Med. Cell. Longev. 2016 (2016) 2183026.
[5] P. Ferdinandy, D.J. Hausenloy, G. Heusch, G.F. Baxter, R. Schulz, Interaction of risk factors, comorbidities, and comedications with ischemia/reperfusion injury and cardioprotection by preconditioning, postconditioning, and remote conditioning, Pharmacol. Rev. 66 (4) (2014) 1142–1174.
[6] D. Li, N. Lu, J. Han, X. Chen, W. Hao, W. Xu, X. Liu, L. Ye, Q. Zheng, Eriodictyol attenuates myocardial ischemia-reperfusion injury through the activation of JAK2, Front. Pharmacol. 9 (2018) 33.
[7] H. Zhou, Q. Ma, P. Zhu, J. Ren, R.J. Reiter, Y. Chen, Protective role of melatonin in cardiac ischemia-reperfusion injury: from pathogenesis to targeted therapy, J. Pineal Res. 64 (3) (2018).
[8] Y. Yang, J. Lv, S. Jiang, Z. Ma, D. Wang, W. Hu, C. Deng, C. Fan, S. Di, Y. Sun, W. Yi, The emerging role of toll-like receptor 4 in myocardial inflammation, Cell Death Dis. 7 (2016) e2234.
[9] J. Ansari, G. Kaur, F.N.E. Gavins, Therapeutic potential of annexin A1 in ischemia reperfusion injury, Int. J. Mol. Sci. 19 (4) (2018).
[10] J.P. Vago, L.P. Tavares, M.A. Sugimoto, G.L. Lima, I. Galvao, T.R. de Caux, K.M. Lima, A.L. Ribeiro, F.S. Carneiro, F.F. Nunes, V. Pinho, M. Perretti, M.M. Teixeira, L.P. Sousa, Proresolving actions of synthetic and natural protease inhibitors are mediated by annexin A1, J. Immunol. 196 (4) (2016) 1922–1932.
[11] C.X. Qin, S.B. Finlayson, A. Al-Sharea, M. Tate, M.J. De Blasio, M. Deo, S. Rosli, D. Prakoso, C.J. Thomas, H. Kiriazis, E. Gould, Y.H. Yang, E.F. Morand, M. Perretti, A.J. Murphy, X.J. Du, X.M. Gao, R.H. Ritchie, Endogenous Annexin-A1 regulates haematopoietic stem cell mobilisation and inflammatory response post myocardial infarction in mice in vivo, Sci. Rep. 7 (1) (2017) 16615.
[12] C. Qin, Y.H. Yang, L. May, X. Gao, A.G. Stewart, Y. Tu, O.L. Woodman, R.H. Ritchie, Cardioprotective potential of annexin-A1 mimetics in myocardial infarction, Pharmacol. Ther. 148 (2015) 47–65.
[13] Z. Boudhraa, C. Merle, D. Mazzocut, J.M. Chezal, C. Chambon, E. Miot-Noirault, M. Theisen, B. Bouchon, F. Degoul, Characterization of pro-invasive mechanisms and N-terminal cleavage of ANXA1 in melanoma, Arch. Dermatol. Res. 306 (10) (2014) 903–914.
[14] A. Wincewicz, S. Sulkowski, Stat proteins as intracellular regulators of resistance to myocardial injury in the context of cardiac remodeling and targeting for therapy, Adv. Clin. Exp. Med. 26 (4) (2017) 703–708.
[15] Y. Yang, W. Duan, Z. Jin, W. Yi, J. Yan, S. Zhang, N. Wang, Z. Liang, Y. Li, W. Chen, D. Yi, S. Yu, JAK2/STAT3 activation by melatonin attenuates the mitochondrial oxidative damage induced by myocardial ischemia/reperfusion injury, J. Pineal Res. 55 (3) (2013) 275–286.
[16] Y.W. Hu, K. Liu, M.T. Yan, Effect and mechanism of icariin on myocardial ischemia-reperfusion injury model in diabetes rats, Zhongguo Zhong Yao Za Zhi 40 (21) (2015) 4234–4239.
[17] Y. Fang, X. Guan, T. Cai, J. Long, H. Wang, X. Xie, Y. Zhang, Knockdown of ANXA1 suppresses the biological behavior of human NSCLC cells in vitro, Mol. Med. Rep. 13 (5) (2016) 3858–3866.
[18] C. Beeton, A. Garcia, K.G. Chandy, Drawing blood from rats through the saphenous vein and by cardiac puncture, J. Vis. Exp. (7) (2007) 266.
[19] X. Long, Q. Chen, J. Zhao, N. Rafaels, P. Mathias, H. Liang, J. Potee, M. Campbell, B. Zhang, L. Gao, S.N. Georas, D. Vercelli, T.H. Beaty, I. Ruczinski, R. Mathias, K.C. Barnes, X. Chen, An IL-13 promoter polymorphism associated with liver fibrosis in patients with *Schistosoma japonicum*, PLoS One 10 (8) (2015) e0135360.
[20] H. Huang, H. Xie, Y. Pan, K. Zheng, Y. Xia, W. Chen, Plumbagin triggers ER stress-mediated apoptosis in prostate cancer cells via induction of ROS, Cell. Physiol. Biochem. 45 (1) (2018) 267–280.
[21] J. Zhang, B. Lian, Y. Shang, C. Li, Q. Meng, miR-135a protects dextran sodium sulfate-induced inflammation in human colorectal cell lines by activating STAT3 signal, Cell. Physiol. Biochem. 51 (3) (2018) 1001–1012.
[22] P. Maiti, A. Al-Gharaibeh, N. Kolli, G.L. Dunbar, Solid lipid curcumin particles induce more DNA fragmentation and cell death in cultured human glioblastoma cells than does natural curcumin, Oxidative Med. Cell. Longev. 2017 (2017) 9656719.
[23] K.J. Livak, T.D. Schmittgen, Analysis of relative gene expression data using real-time quantitative PCR and the 2(−Delta Delta C(T)) method, Methods 25 (4) (2001) 402–408.
[24] A.I. Rojo, O.N. Medina-Campos, P. Rada, A. Zuniga-Toala, A. Lopez-Gazcon, S. Espada, J. Pedraza-Chaverri, A. Cuadrado, Signaling pathways activated by the phytochemical nordihydroguaiaretic acid contribute to a Keap1-independent regulation of Nrf2 stability: role of glycogen synthase kinase-3, Free Radic. Biol. Med. 52 (2) (2012) 473–487.
[25] R. de Jong, G. Leoni, M. Drechsler, O. Soehnlein, The advantageous role of annexin A1 in cardiovascular disease, Cell Adhes. Migr. 11 (3) (2017) 261–274.
[26] V. Bizzarro, R. Belvedere, V. Migliaro, E. Romano, L. Parente, A. Petrella, Hypoxia regulates ANXA1 expression to support prostate cancer cell invasion and aggressiveness, Cell Adhes. Migr. 11 (3) (2017) 247–260.
[27] K.M. Lima, J.P. Vago, T.R. Caux, G.L. Negreiros-Lima, M.A. Sugimoto, L.P. Tavares, R.G. Arribada, A.A.F. Carmo, I. Galvao, B.R.C. Costa, F.M. Soriani, V. Pinho, E. Solito, M. Perretti, M.M. Teixeira, L.P. Sousa, The resolution of acute inflammation induced by cyclic AMP is dependent on annexin A1, J. Biol. Chem. 292 (33) (2017) 13758–13773.
[28] V. Bizzarro, R. Belvedere, M.R. Milone, B. Pucci, R. Lombardi, F. Bruzzese, A. Popolo, L. Parente, A. Budillon, A. Petrella, Annexin A1 is involved in the acquisition and maintenance of a stem cell-like/aggressive phenotype in prostate cancer cells with acquired resistance to zoledronic acid, Oncotarget 6 (28) (2015) 25076–25092.
[29] H.H. Su, Y.C. Chu, J.M. Liao, Y.H. Wang, M.S. Jan, C.W. Lin, C.Y. Wu, C.Y. Tseng,

J.C. Yen, S.S. Huang, Phellinus linteus mycelium alleviates myocardial ischemia-reperfusion injury through autophagic regulation, Front. Pharmacol. 8 (2017) 175.
[30] S. Cadenas, ROS and redox signaling in myocardial ischemia-reperfusion injury and cardioprotection, Free Radic. Biol. Med. 117 (2018) 76–89.
[31] T. Wang, X. Mao, H. Li, S. Qiao, A. Xu, J. Wang, S. Lei, Z. Liu, K.F. Ng, G.T. Wong, P.M. Vanhoutte, M.G. Irwin, Z. Xia, N-Acetylcysteine and allopurinol up-regulated the Jak/STAT3 and PI3K/Akt pathways via adiponectin and attenuated myocardial postischemic injury in diabetes, Free Radic. Biol. Med. 63 (2013) 291–303.
[32] B. Crowe, J.A. Poynter, M.C. Manukyan, Y. Wang, B.D. Brewster, J.L. Herrmann, A.M. Abarbanell, B.R. Weil, D.R. Meldrum, Pretreatment with intracoronary mimosine improves postischemic myocardial functional recovery, Surgery 150 (2) (2011) 191–196.
[33] J. Yang, L. Guo, R. Liu, H. Liu, Neuroprotective effects of VEGF administration after focal cerebral ischemia/reperfusion: dose response and time window, Neurochem. Int. 60 (6) (2012) 592–596.
[34] J. Han, D. Wang, L. Ye, P. Li, W. Hao, X. Chen, J. Ma, B. Wang, J. Shang, D. Li, Q. Zheng, Rosmarinic acid protects against inflammation and cardiomyocyte apoptosis during myocardial ischemia/reperfusion injury by activating peroxisome proliferator-activated receptor gamma, Front. Pharmacol. 8 (2017) 456.
[35] R. Li, L. Fan, F. Ma, Y. Cao, J. Gao, H. Liu, Y. Li, Effect of etomidate on the oxidative stress response and levels of inflammatory factors from ischemia-reperfusion injury after tibial fracture surgery, Exp. Ther. Med. 13 (3) (2017) 971–975.
[36] J. Kim, J. Kim, H. Kook, W.J. Park, PICOT alleviates myocardial ischemia-reperfusion injury by reducing intracellular levels of reactive oxygen species, Biochem. Biophys. Res. Commun. 485 (4) (2017) 807–813.
[37] A. Kiani-Esfahani, S. Kazemi Sheykhshabani, M. Peymani, M.S. Hashemi, K. Ghaedi, M.H. Nasr-Esfahani, Overexpression of annexin A1 suppresses pro-inflammatory factors in PC12 cells induced by 1-Methyl-4-Phenylpyridinium, Cell J. 18 (2) (2016) 197–204.
[38] L. Liu, D. An, J. Xu, B. Shao, X. Li, J. Shi, Ac2-26 induces IKKbeta degradation through chaperone-mediated autophagy via HSPB1 in NCM-treated microglia, Front. Mol. Neurosci. 11 (2018) 76.
[39] Q. Xia, X. Li, H. Zhou, L. Zheng, J. Shi, S100A11 protects against neuronal cell apoptosis induced by cerebral ischemia via inhibiting the nuclear translocation of annexin A1, Cell Death Dis. 9 (6) (2018) 657.
[40] D. Pupjalis, J. Goetsch, D.J. Kottas, V. Gerke, U. Rescher, Annexin A1 released from apoptotic cells acts through formyl peptide receptors to dampen inflammatory monocyte activation via JAK/STAT/SOCS signalling, EMBO Mol. Med. 3 (2) (2011) 102–114.
[41] L.S. Torres, J.V. Okumura, D.G. Silva, K.K. Mimura, E. Belini-Junior, R.G. Oliveira, C.L. Lobo, S.M. Oliani, C.R. Bonini-Domingos, Inflammation in sickle cell disease: differential and down-expressed plasma levels of annexin A1 protein, PLoS One 11 (11) (2016) e0165833.
[42] M.A. Sugimoto, J.P. Vago, M.M. Teixeira, L.P. Sousa, Annexin A1 and the resolution of inflammation: modulation of neutrophil recruitment, apoptosis, and clearance, J. Immunol. Res. 2016 (2016) 8239258.
[43] A. Das, F.N. Salloum, D. Durrant, R. Ockaili, R.C. Kukreja, Rapamycin protects against myocardial ischemia-reperfusion injury through JAK2-STAT3 signaling pathway, J. Mol. Cell. Cardiol. 53 (6) (2012) 858–869.
[44] Y.J. Kim, J.M. Shin, S.H. Shin, J.H. Kim, K.Y. Sohn, H.J. Kim, J.K. Kang, S.Y. Yoon, J.W. Kim, 1-palmitoyl-2-linoleoyl-3-acetyl-rac-glycerol ameliorates arthritic joints through reducing neutrophil infiltration mediated by IL-6/STAT3 and MIP-2 activation, Oncotarget 8 (57) (2017) 96636–96648.
[45] L.C. Tong, Y. Wang, Z.B. Wang, W.Y. Liu, S. Sun, L. Li, D.F. Su, L.C. Zhang, Propionate ameliorates dextran sodium sulfate-induced colitis by improving intestinal barrier function and reducing inflammation and oxidative stress, Front. Pharmacol. 7 (2016) 253.